

Interface magnetism and electronic structure: ZnO(0001)/Co₃O₄(111)I.M. Kupchak,¹ N.F. Serpak,¹ A. Shkrebtiy,² and R. Hayn³¹*V.Lashkarev Institute of Semiconductor Physics, NAS Ukraine, 45, Pr. Nauky, Kyiv, 03680, Ukraine*^{a)}²*University of Ontario, Institute of Technology, 2000 Simcoe Street North, Oshawa, Ontario L1H 7K4, Canada*³*Aix-Marseille Université, CNRS, IM2NP-UMR 7334, 13397 Marseille Cedex 20, France*

(Dated: 13 November 2018)

We have studied the structural, electronic and magnetic properties of spinel Co₃O₄ (111) surfaces and their interfaces with ZnO (0001) using density functional theory (DFT) within the Generalized Gradient Approximation with on-site Coulomb repulsion term (GGA+U). Two possible forms of spinel surface, containing Co²⁺ or Co³⁺ ions and terminated with either cobalt or oxygen ions were considered, as well as their interface with zinc oxide. Our calculations demonstrate that Co³⁺ ions attain non-zero magnetic moments at the surface and interface, in contrast to the bulk, where they are not magnetic, leading to the ferromagnetic ordering. Since heavily Co-doped ZnO samples can contain Co₃O₄ secondary phase, such a magnetic ordering at the interface might explain the origin of the magnetism in such diluted magnetic semiconductors (DMS).

PACS numbers: 73.20.-r, 75.70.-i

Keywords: spinel; cobalt oxide; zinc oxide; diluted magnetic semiconductors; cobalt spinel surfaces, cobalt spinel – zinc oxide interfaces; interface magnetism;

^{a)}Electronic mail: kupchak@isp.kiev.ua

CONTENTS

I. Introduction	2
II. Numerical Method	6
III. Surface and interface structural details	7
IV. Results and discussion	9
V. Conclusion	16
Acknowledgments	16
References	17

I. INTRODUCTION

Magnetic semiconductors (MS) and diluted magnetic semiconductors (DMS) exhibit both ferromagnetic and semiconducting properties. Therefore, they are promising materials for spintronics, which utilizes for information processing not only the electron charge but also its spin. Historically, the first DMS with a high Curie temperature up to about 200 K was GaAs doped with Mn ions.^{1,2} In that compound, the ferromagnetism is promoted by hole carriers, which align along the local Mn magnetic moments and called carrier-induced ferromagnetism or Zener $p - d$ exchange. It is crucial for this mechanism that Mn at the Ga site becomes Mn^{2+} instead of Ga^{3+} , thus providing at the same time a local spin and a hole charge carrier. Extension of the mechanism, proposed in a very influential paper³ of Dietl and co-workers, allows a prediction that the above room-temperature ferromagnetism in ZnO:Co and GaN:Mn is due to the same carrier-induced mechanism. This would be responsible for the ferromagnetism with a sufficiently high number of hole charge carriers. First experiments after that prediction⁴ seemed to confirm the mechanism proposed and has also been supported by *ab-initio* calculations.⁵ However, it soon turned out that the Co impurity is in fact isovalent to the Zn ion⁶ and provides no charge carriers at all, while the situation in GaN:Mn is similar.⁷

We are going to concentrate here on ZnO:Co , where the experimental reports demon-

strate that the above room-temperature ferromagnetism in ZnO:Co persist. Even though its origin is still not clarified, there are clear indications in more recent experiments that the magnetism in the ZnO:Co system is attributed to the formation of the Co_3O_4 phase in ZnO.⁸⁻¹² Therefore, we will focus here on the role of the Co_3O_4 phase, although several attempts to explain the mechanism of the ferromagnetism in realistic ZnO:Co systems exist including, for instance, spinodal decomposition¹³ or Lieb-Mattis ferrimagnetism,¹⁴ to cite just two ideas.

The typical doping level of Co in ZnO can be relatively high (in the range between 10% and 30%). This leads to the secondary phases of Co_3O_4 and ZnCo_2O_4 segregation during the sample growth, which can be detected, for instance, by Raman spectroscopy.^{15,16} Although, in general, the appearance of such secondary phases is detrimental for the DMS materials, this effect can also be advantageous. However, a lack of understanding of the secondary phases and their interfaces remains currently the main obstacle toward the practical applications of Co_3O_4 surfaces and their interfaces. By carrying out the first principle simulations of the $\text{Co}_3\text{O}_4/\text{ZnO}$ interface we offer not only the realistic explanations in the big puzzle of the nature of ferromagnetism in DMS, but also show the promise for the new applications.

Cobalt oxide Co_3O_4 , also known as tricobalt tetraoxide or cobalt spinel, is a *p*-type semiconductor with the reported optical energy band gap E_g between 1.1 and 1.65 eV (see [17] and ref. therein). It is widely used in lithium-ion batteries as a cathode material,¹⁸ gas sensing, nanomaterials and nano-junctions, environmental and numerous other applications.¹⁹⁻²² Co_3O_4 crystallizes in the cubic normal spinel structure, which contains cobalt ions in two different oxidation states, Co^{2+} and Co^{3+} , located at the interstitial tetrahedral (A) and octahedral (B) sites, respectively (see., *e.g.*, Ref. [17]). The bulk magnetic properties of the cobalt oxide are well understood. In the presence of tetrahedral crystal field, the five-fold degenerate atomic *d* orbitals of Co^{2+} ions are split into two groups, e_g and t_{2g} , leading to three unpaired *d* electrons on t_{2g} orbital. Similarly, in a case of Co^{3+} ion, the crystal field is octahedral, and the splitting leads to six paired electrons in the t_{2g} orbital, while e_g orbital is empty. As a result, the Co^{2+} ions carry a permanent magnetic moment, whereas Co^{3+} ions are not magnetic. Considering the A-site sublattice only, each Co^{2+} ion is surrounded by four neighbors with oppositely directed spin, thus forming an antiferromagnetic (AFM) state. In general, such nearest A-A exchange interaction is expected to be weak, since in the typical spinel structures with magnetic cations A-B coupling between the ions in tetra-

hedral and octahedral sites is dominant.²³ However, in the Co_3O_4 spinel this A-A coupling is unusually strong due to the indirect exchange through the intermediate Co^{3+} ions in the octahedral B-site, providing Co^{2+} ions by a magnetic moment of about $3.02 \mu_B$. As a result of such strong coupling, Co_3O_4 is antiferromagnetic below the Néel temperature $T_N \sim 40 \text{ K}$ and paramagnetic at higher temperatures.²³

When such a complex structure is terminated by a surface or forms an interface, one can expect new interesting magnetic peculiarities, absent in the bulk of the crystal. Indeed, formation of surface or interface between different materials involves several important factors such as surface polarity, charge transfer, stresses, defects, *etc.*, altering the long-range magnetic ordering, and the magnetic response as a result.^{24,25} There are many publications on the electronic and magnetic properties of different spinels and their surfaces, such as Fe_3O_4 spinel (see, *e.g.*, [25]), which has the crystal structure similar to that of Co_3O_4 . However, the cobalt spinel surfaces are still not that well understood, while even more complex behaviour should be expected when the interface with other materials is formed. It has been shown that during the epitaxial growth of Co_3O_4 , two surfaces with the lowest surface energy, namely (111) and (110), are typically formed.²⁶ More detailed experimental and theoretical study have been performed in [27], where the effect of different Co_3O_4 crystal planes orientation has been investigated. This aimed in reducing charge-discharge over-potential toward an application in high energy density Li – O_2 batteries and it was established, that (111) surface is the most efficient. Experimentally, cobalt spinel (110) surface has been thoroughly investigated by Petitto and Langel²⁸ using low energy electron diffraction (LEED), Auger electron spectroscopy (AES), and X-ray photoelectron spectroscopy (XPS). The Co_3O_4 (111) surface has been studied by X-ray diffraction (XRD) and atomic force microscopy (AFM) methods,²⁹ LEED and scanning tunneling microscopy (STM).^{30–33} Bulk Co_3O_4 have also been studied using Raman spectroscopy.³⁴ In general, Co_3O_4 attracts the interest because of its high catalytic activity, especially for CO oxidation,³⁵ therefore most of the research have been performed toward such an application. Concerning the theory, a number of publications has been dedicated to *ab-initio* study of electronic and magnetic properties of the bulk and surfaces of Co_3O_4 .^{36–43} The main problem, discussed in the above cited theoretical works, was usually a nature of superexchange in bulk spinel and the stability of its surfaces under different conditions, such as different atom types (Co^{2+} , Co^{3+} ions, or O) at the top layer termination.

Another field of cobalt spinel application is related to the interface between p -type Co_3O_4 and n -type ZnO , which forms p - n heterojunction. In particular, p - $\text{Co}_3\text{O}_4/n$ - ZnO composites can provide higher sensitivities and faster responses toward gas sensing application.^{21,44–47} Such composites are typically obtained using a mixture of ZnO and Co_3O_4 powders and following annealing, that forms inhomogeneous interface between both semiconductors. However, the presence of this interface also plays a significant role in the magnetic properties of such composites. Indeed, there is an evidence of the magnetism appearance in $\text{ZnO}/\text{Co}_3\text{O}_4$ powder mixture at room temperature even without thermal treatment.^{48,49} Authors explain this phenomena by surface reduction of the Co_3O_4 nanoparticles, in which the antiferromagnetic Co_3O_4 nanoparticle is surrounded by a CoO -like shell. Other authors,^{50,51} studying $\text{ZnO}/\text{Co}_3\text{O}_4$ powder mixture by X-ray absorption spectroscopy (XAS) and optical spectroscopy, explained such phenomena by reduction $\text{Co}^{3+} \rightarrow \text{Co}^{2+}$ at the Co_3O_4 nanoparticle surface. This explanation has been proved by Vibrating Sample Magnetometer (VSM) analysis of composite ZnO , synthesized on the surface of core Co_3O_4 in [52]. Recently a diode consisting of p -type Co_3O_4 nanoplate / n -type ZnO nanorods heteroepitaxial junction has been fabricated, showing reasonable electrical performance,⁵³ but no attention has been paid to its magnetic properties. Despite of extensive investigation of the cobalt oxides, mentioned above, still there is no clear picture of the role of the cobalt oxide surfaces and interfaces on the magnetic properties.

Considering the lack of microscopic understanding of the surface and interface magnetism, the present study is aimed to establish the nature of ferromagnetism at the $\text{Co}_3\text{O}_4/\text{ZnO}$ interface toward an application in the new device types for spintronics. We have investigated from first principles modifications of the atomic structure at various types of the $\text{Co}_3\text{O}_4/\text{ZnO}$ boundaries, related changes in the electronic band structure and their contribution to the appearance of the interface magnetic properties. The paper is organized as following. We present in Section 2 the numerical formalism, which is used throughout the paper. Section 3 discusses the microscopic atomic structure of the $\text{Co}_3\text{O}_4(111)$ surfaces and $\text{Co}_3\text{O}_4/\text{ZnO}$ interfaces. The results of the calculated magnetic and electronic properties and their modifications due to the surfaces or interfaces, are discussed in Section 4. The conclusion is presented in Section 5.

II. NUMERICAL METHOD

We investigated the atomic and electronic structure of the $\text{Co}_3\text{O}_4/\text{ZnO}$ interface within the density functional theory (DFT) and generalized gradient approximation (GGA), as implemented in the Quantum-Espresso software package.⁵⁴ We have used ultrasoft Perdew-Burke-Ernzerhof (PBE) pseudopotentials,⁵⁵ which include 12 valence electrons for zinc, 6 valence electrons for oxygen, and 9 valence electrons for cobalt. An integration of the Brillouin zone has been performed using 4×4 Γ -centered grid of special points in k -space, generated by Monkhorst-Pack scheme⁵⁶ and Methfessel-Paxton smearing⁵⁷ with a parameter of 0.005 Ry. Several tests were performed with denser grids up to 10×10 , but no significant changes have been observed compared to the case of 4×4 grid. To ensure a sufficient convergence of the results we applied 40 Ry cutoff for smooth part of the wave function and 400 Ry for the augmented charge density. We approximated the exchange-correlation functional with both the local spin resolved generalized gradient approximation (SGGA) and the so-called SGGA+U approximation, in which the effect of electron correlations in the $3d$ shell is taken into account by considering the on-site Coulomb interactions within the Hubbard method.^{38,58} We have chosen the value of Hubbard U parameters to be 3.5 eV and 5.0 eV for Co and Zn atoms, respectively.

Although the Hubbard parameters chosen are commonly accepted in the literature, they still are a subject of discussion.³⁸ Therefore, DFT+U calculations of Co_3O_4 should be carried out with care: the systems under consideration might have several solutions and there is no guarantee whether the lowest energy solution corresponds to the global minimum. For such a reason, we have checked that our conclusions do not depend in a sensitive way on these Coulomb parameters. As discussed in [58], the DFT+U instability can be further exacerbated in the presence of the f -orbitals and the absence of the gap between the filled and empty states. However, considered here surfaces and interfaces are semiconducting and the f -states are not present. To make sure that the Coulomb parameters choice does not affect our results, we followed the established approach from [40]. In particular, (i) we applied a Methfessel-Paxton smearing technique of the Brillouin-zone integration that, as proved, ensures the convergence to the global minimum both for metals and systems with nonzero energy gap. (ii) We have also considered several different values of the Hubbard parameter and found that the calculations consistently converges to the same energy.

To optimize the atomic geometry of Co_3O_4 surfaces and $\text{Co}_3\text{O}_4/\text{ZnO}$ interfaces we have performed the structural relaxations within the SGGA method, while the final calculations of the magnetic structure and the densities of states has been carried out using the SGGA+U method. The systems were relaxed through all the internal coordinates until the Hellmann-Feynman forces became less than 10^{-4} a.u., while keeping the shape and the volume of the supercell fixed.

III. SURFACE AND INTERFACE STRUCTURAL DETAILS

To investigate the origin of the surface/interface magnetism we model two types of $\text{Co}_3\text{O}_4(111)$ surfaces and two $\text{ZnO}(0001)/\text{Co}_3\text{O}_4(111)$ interfaces. While the above considered surfaces and interfaces are well suited to simulate numerically, in addition to (111) planes differently oriented interfaces were observed experimentally.^{26,44,46,59,60} However, as we discuss below, the main magnetic features, predicted for (111) system considered, should also be common for differently oriented interfaces in the experimentally observed materials.

The bulk terminated atomic structure of $\text{Co}_3\text{O}_4(111)$ spinel surface in [111] direction, perpendicular to the surface, can be described by a sequence of atomic layers, containing Co^{2+} ions or both of Co^{2+} and Co^{3+} ions, separated by layer of oxygen: $\text{O} - \text{Co}^{2+} - \text{O} - \text{Co}^{2+}\text{Co}^{3+}$. The primitive unit cell, containing such a sequence, has a hexagonal symmetry along the surface or the interface. The upper layer, which forms the interface with ZnO, contains either three Co^{3+} ions (B-terminated layer) or a combination of two Co^{2+} and one Co^{3+} ions (A-terminated layer, such convention is used since the closest to the interface cobalt oxide layer is of A-type). The interface between the upper layer of Co_3O_4 and ZnO is then being formed by introducing a single layer of four oxygen atoms, which match the Co–O bonds of the spinel. These four oxygen atoms can also be viewed as those belonging to ZnO in a sequence $\text{Zn} - \text{O} - \text{Zn} - \text{O}$ of the primitive unit cell: the topology of this spinel oxygen layer has the same symmetry as (0001) plane of hexagonal ZnO. Hence, to form the epitaxial interface with Co_3O_4 and to saturate these oxygen bonds, four primitive unit cells of hexagonal ZnO are required. In such a way, oxygen atoms play a role of a “bridge” between cubic spinel Co_3O_4 and wurtzite ZnO.

We have paid special attention when choosing the lateral unit cell size of the interface for the systems under investigation since $\text{Co}_3\text{O}_4(111)$ and $\text{ZnO}(0001)$ demonstrate considerable

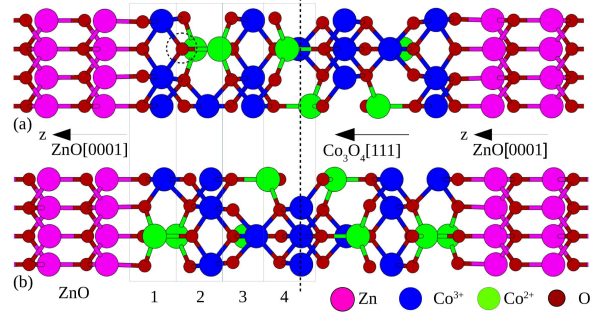


FIG. 1. (Color online) Side view of the unit cells of $\text{Co}_3\text{O}_4/\text{ZnO}$ interfaces: (a) “Octahedral” B-terminated interface, (b) “Tetrahedral” A-terminated interface. Numbers denote the atomic layers of both interfaces.

lattice mismatch. To simulate the $\text{ZnO}(0001)/\text{Co}_3\text{O}_4(111)$ interface three possibilities exist: (i) choosing the spinel bulk constant to determine the interface unit cell size, (ii) using ZnO bulk parameters to define the interface unit cell, and (iii) optimizing the lattice parameter for the interface to find the unit cell size that minimizes the total energy of the interface. Following the experimental finding, we did not optimize the lattice parameter for the interface, since such optimization should lead to both ZnO and Co_3O_4 material stressed. Indeed, for our case, while such mismatch should make the epitaxial growth of the flat $\text{Co}_3\text{O}_4/\text{ZnO}$ interface challenging, the experimental microscopic images demonstrate the smooth interface between Co_3O_4 inclusions and ZnO host material^{44,46,59} without noticeable modification of the interlayer distances and dislocation appearance. Since Co_3O_4 is supposed to be the source of the magnetism, first we have chosen spinel bulk constant as the main structural parameter, resulted in compressed ZnO part of the system, and then relaxed the atomic positions in the interface vicinity. Considering the experimental value of bulk spinel lattice constant $a_{\text{spinel}} = 8.084 \text{ \AA}$, a primitive unit cell of its (111) surface has a lattice constant $c_{\text{spinel}} = 5.72 \text{ \AA}$. Since the corresponding parameter of ZnO has a value $c_{\text{ZnO}} = 3.25 \text{ \AA}$, in order to fit four primitive unit cells of ZnO onto single 2D unit cell of spinel, the bulk constant of ZnO should be compressed in the basal plane by about 12%. Therefore, the lattice constant of this strained ZnO at the interface region is 2.86 \AA . As it has been suggested in [53] for ZnO nanorods on Co_3O_4 nanoplates, such a large stress is relieved by forming dislocations along basal plane at the interface. In the case of the Co_3O_4 inclusions, however, they have low-sized diameters, which allow to easily accommodate the strain through

the lateral relaxation, thus making heteroepitaxial growth possible even in the case of high lattice mismatch.³⁵ Additionally, in the present calculations such a stress effect is partially taken into account by the system relaxation within the unit cell. On the other hand, study of possible extended dislocations, originated due to the mismatch, requires simulation of significantly larger unit cells and was out of the scope of our research.

Second, we have chosen to test the ZnO unit cell size for the interface, which resulted in “stretched” Co₃O₄ side. However, when we carried out the relaxation of the atomic positions in the interface vicinity, the spinel-like structure of Co₃O₄ has not been preserved. Again, considering the experimental finding of the bulk-like Co₃O₄ spinel inclusions on XRD spectra⁶¹, existence of such stretched Co₃O₄ systems does not look credible. To confirm this conclusion we again compared our theoretical results with the experimental Raman spectra, as discussed below.

Therefore, to study magnetic and electronic structures of an interface, we created two symmetric slabs, containing seven atomic layers of Co₃O₄, and ZnO layers, adjacent on both sides, as shown in Fig. 1. The first slab (Fig. 1a) is composed of a spinel top layer containing Co³⁺ ions at the B-sites only (“octahedral” interface), while the second slab (Fig. 1b) contains at the interface both Co²⁺ (A-site) and one Co³⁺ (B-site) ions (“tetrahedral” interface). In such a way, each slab contains two interface regions of the same symmetry (topology), so their total dipole moment is close to zero. The ZnO part of the slab is two lattice constants c_{ZnO} thick on both sides and 12 Å of vacuum layer have been added to separate the slabs in z direction. Additionally, we have studied the bulk spinel properties, using the $12 \times 12 \times 12$ k -point grid, and its clean (111) surface within the same method. We simulated the Co-terminated and O-terminated spinel (111) surfaces using the slabs, created for the interface model, but with ZnO layers removed and followed by subsequent relaxation over all coordinates.

IV. RESULTS AND DISCUSSION

We constructed the interface and surface models assuming that the secondary phase preserves bulk spinel crystal structure with the corresponding bulk constant. Our assumption is based on the comparison with the Raman spectra calculated⁶² and measured^{34,61} for both Co₃O₄ and Zn_{1-x}Co_xO. In general, the symmetry of the bulk spinel unit cell is described by

point group $\Gamma(O_h^7)$,⁶³ and therefore the phonon normal modes near the Brillouin zone center may be obtained by the decomposition $\Gamma(O_h^7) = A_{1g} + E_g + 3F_{2g} + 5F_{1u} + 2A_{2u} + 2E_u + 2F_{2u}$. Here A_{1g} , E_g and triple degenerated $3F_{2g}$ modes are Raman active. We calculated the frequencies of these phonon modes for bulk spinel with lattice constant $a_{spinel} = 8.084 \text{ \AA}$ (corresponding to the case of normal spinel secondary phase and compressed ZnO at the interface), and “stretched” spinel using experimental ZnO bulk constant, which leads to $a_{spinel} = 9.191 \text{ \AA}$, using density-functional perturbation theory.⁶⁴ The PBE pseudopotentials were selected in norm-conserving form, the wave function expansion cutoff of 80 Ry and $4 \times 4 \times 4$ k-point grid for Brillouin zone integration were adopted for this calculations. The calculated and measured Raman frequencies are collected in Table I. It demonstrates that the calculated Raman spectra are very sensitive to the choice of the lattice constant. Frequencies obtained in both LDA and GGA approximations for normal spinel are comparable with measured ones, while those calculated for “stretched” spinel are found to be significantly lower and are not observed experimentally. Moreover, XRD measurements of $\text{Zn}_{1-x}\text{Co}_x\text{O}$ ⁶¹ do not indicate a presence of any other structures beside of ZnO and ZnCo_2O_4 . The above comparison of the theoretical and experimental frequencies is in favor of using the bulk Co_3O_4 constant when modeling the interface with ZnO.

The calculated lattice constant for bulk spinel $a_{spinel} = 8.147 \text{ \AA}$, and the corresponding interplanar A-B spacing $d_{111} = 2.351 \text{ \AA}$ are overestimated by only 0.8% compared to the experimental values of $a_{spinel} = 8.084 \text{ \AA}$ and $d_{111} = 2.333 \text{ \AA}$, respectively. Therefore, we used the experimental spinel bulk constant.

TABLE I. Raman-active bulk phonon modes of Co_3O_4 , cm^{-1} . Two last lines show the frequencies, calculated in this study

	F_{2g}	E_g	F_{2g}	F_{2g}	A_{1g}
Co_3O_4 [Ref. ³⁴]	194.4	482.4	521.6	618.4	691.0
$\text{Zn}_{1-x}\text{Co}_x\text{O}$ [Ref. ⁶¹]		486	524	623	710
Co_3O_4 LDA [Ref. ⁶²]	192	480	511	589	644
Co_3O_4 GGA	187.0	463.9	502.8	574.5	631.7
stretched Co_3O_4 GGA	62.3	175.4	236.8	325.2	383.8

As mentioned in Sec.3, the unit cell of the spinel (111) plane in the slab construction is

hexagonal, and therefore 4 unit cells of ZnO (also hexagonal) are needed to match one spinel unit cell. Consequently, the planar lattice constant of adjacent ZnO $a_{\text{ZnO}} = 2.88 \text{ \AA}$ is scaled to the spinel lattice constant and cannot be optimized separately. However, the interplanar distances (in z direction) are optimized, for both the spinel and the wurtzite regions of the interface. Therefore, the calculated value of the interplanar spacing at the spinel region of the interface becomes $d_{111} = 2.387 \text{ \AA}$, which is about 2% larger than the experimental bulk interplanar distance, while the lattice constant, calculated for ZnO regions, $c_{\text{ZnO}} = 5.52 \text{ \AA}$, which is about 5% above the corresponding experimental bulk value of 5.27 \AA . These relaxations absorb part of the stress due to the lattice mismatch between spinel and wurtzite. The optimized supercells of $\text{Co}_3\text{O}_4/\text{ZnO}$ interfaces are shown in Fig. 1. Since there are no dangling bonds at the interfaces and all the ions are located in such a way that the bulk crystalline symmetry is preserved, no significant modifications in a topology of adjacent atomic layers were found during the relaxation. In the case of surfaces, there exist four possibilities: B- or A-termination with Co or O top layer. The B-terminated sample with Co top layer demonstrates atomic reordering: the oxygen atom of the second layer (O atom circled by dashed line in Fig. 1a) moves in z -direction to be in the same plane as the Co atoms of first layer. Such reordering occurs in Co^{3+} -terminated surface only: A-terminated surfaces with both Co and O top layers and B-terminated with O top layer demonstrate stable surface topology with no significant changes of the overall atomic positions compared to those in the interfaces. We have also performed geometry optimization for 9 atomic layer - thick Co_3O_4 slabs, and found that the results are practically identical to the case, considered in Fig. 1.

TABLE II. Magnetic moments μ (in the units of μ_B) and charges ρ of Co ions (in a.u.), calculated using Löwdin charge analysis, for octahedral surfaces and interfaces.

		Co-terminated	O-terminated	ZnO	Bulk
		surface	surface	interface	
Co^{3+}	μ	2.33	0.71	0.21	0.0
	ρ	0.94	1.17	1.07	1.02
Co^{2+}	μ	2.45	2.48	2.46	2.59
	ρ	1.16	1.23	1.21	1.22

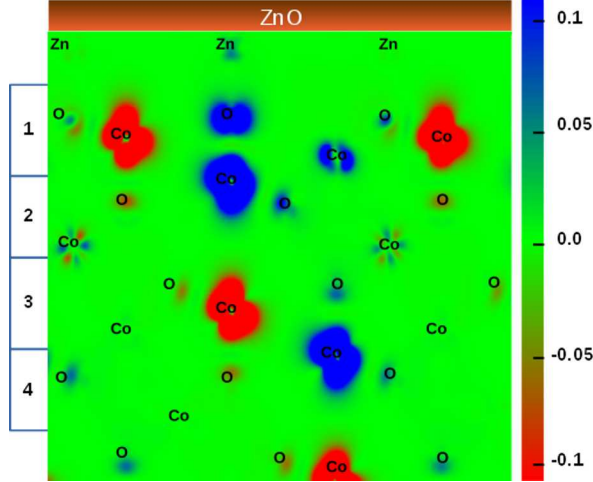


FIG. 2. Spin density distribution for octahedral interface, plotted over vertical $(1\bar{1}0)$ plane. The scale, shown at the right, has units of μ_B . At the left, 1, 2, 3 and 4 stand for the Co_3O_4 interface layer numbers. Chemical symbols indicate the positions of corresponding ions.

It has been discussed above that in the bulk spinel Co^{3+} ions are non-magnetic due to the large splitting between t_{2g} and e_g orbitals, caused by the presence of octahedral crystal field. Since this symmetry is broken at the surface or interface, the electrons could occupy t_{2g} and e_g orbitals in different order, leading to the changes in magnetic properties, as reported in [40,50]. It is important to stress that similar symmetry changes are typical for other Co_3O_4 interface orientations, therefore the results for the $\text{Co}_3\text{O}_4(111)$ surface, considered here, should reflect general trends in the interface induced magnetism origin. To quantify these changes, we calculated and compared the magnetic moment of Co ions for different interface and surface systems using a Löwdin charge analysis. Table II shows the largest values of magnetic moments, calculated for the bulk Co_3O_4 , interfaces and surfaces, both Co- and O-terminated. The magnetic moments for Co^{3+} ions are calculated for the top layer and for Co^{2+} ions in the second layer of octahedral interface or surface. The deviation of the magnetic moment of the same ion type on different sites is relatively small $\sim 0.02 \mu_B$ for all systems, so such values are reflecting the general physical picture.

The calculated magnetic moment of Co^{2+} ions in bulk spinel is $2.59 \mu_B$ is slightly smaller in the case of all considered surfaces, as it is seen from Table II. Instead, while the magnetic moment of Co^{3+} ions is zero in the bulk, it is non-vanishing in the case of the surface. The largest magnetic moment of $2.33 \mu_B$ occurs at the Co-terminated surface, where the bulk

symmetry is broken and ion coordination number is reduced at the most. If the surface is O-terminated, the magnetic moment of Co^{3+} ions reduces to $0.71 \mu_B$, while the external oxygen atoms receive a magnetic moment of $0.34 \mu_B$ due to a strong polarization of the p -orbitals. The charge, calculated for Co^{3+} ions in the bulk, is about 0.2 a.u. larger than that one of Co^{2+} , as shown in Table II. These values differ slightly for all of the systems under study, and, in general, we have to introduce new oxidation state types for Co ions in interfaces and surfaces. However, in our calculations the charge of Co^{3+} is always larger than that of Co^{2+} , and this fact allow us, for the sake of simplicity, to use explicit “bulk” notations Co^{2+} and Co^{3+} for corresponding ions in all of systems. The spin density distribution for tetrahedral interface is shown in Fig. 2. The blue and red colors regions around the Co^{2+} ions of the Layers 1 and 3 indicate the presence of magnetic moment, comparable to that in the bulk. Co^{3+} ions of the Layers 3 and 4 are completely bare, that is spin compensated, but receive small magnetic moment in Layer 2, which becomes noticeably larger at the interfacing layer. Similarly to the case of O-terminated surface, one of oxygen ions acquires a magnetic moment of $0.22 \mu_B$, as indicated by blue colour. Obviously, such a magnetic ordering corresponds to AFM state: we calculated the total energy for the different spin orientations, and for this tetrahedral interface the difference between the energies of ferromagnetic (FM) and antiferromagnetic (AFM) states is $E_{\text{FM}} - E_{\text{AFM}} = 94 \text{ meV}$. For the octahedral interface FM state is energetically preferable and the difference in energy between FM and AFM states is -23 meV . In general, the lowest total energy is found for octahedral interface with FM magnetic ordering.

More accurate method to estimate the relation between the interface type and magnetic ordering is to calculate the formation energy. Such an approach, however, requires the knowledge of the chemical potentials of participating ions. To the best of our knowledge such problem has not been solved yet: the main challenge is to properly find these potentials for ions in different oxidation states.

It is worth to note, that the magnetic moments were calculated for the relaxed systems while keeping the C_{3v} symmetry intact. If this symmetry is broken (for instance, for differently oriented interfaces or when the initial deviations from equilibrium positions are different for symmetry equivalent atoms, or due to defects), the corresponding magnetic moments might differ slightly. Nevertheless, the general picture should remain the same: Co^{3+} ions are gaining the non-zero magnetic moments both at the surface and interface, in

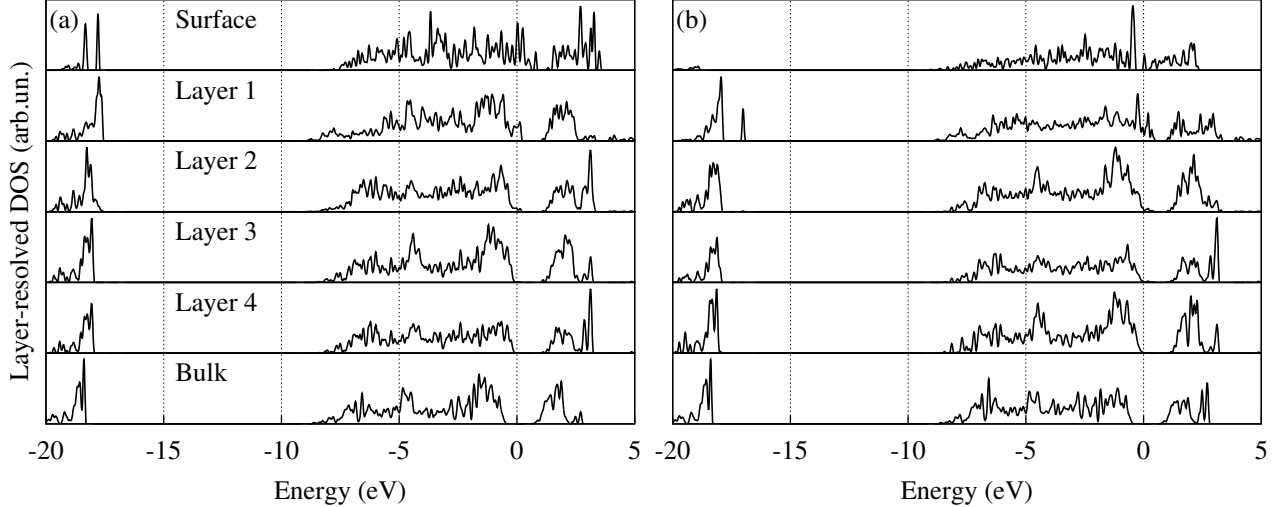


FIG. 3. Layer-resolved DOS of (a) octahedral and (b) tetrahedral spinel (111) surfaces and (111) spinel / (0001) wurtzite interfaces. From top to bottom: top layer of spinel (111) surface with no ZnO cap; layers 1 to 4 of the spinel structure close to the spinel/wurtzite interface and the layer-resolved DOS for the (111) plane of bulk spinel (see discussions in the text).

contrast to the bulk case. Therefore, the magnetic effects, discussed above, should also be present for differently oriented parts of the Co_3O_4 inclusions.

As it is known, a presence of the dangling bonds leads to additional surface states, observable in the density of states (DOS). Formation of the interface between two different materials is also responsible for the interface states, localized close to the boundary between the two materials. The surface or interface formation causes the charge redistribution and change in the corresponding magnetic properties. To demonstrate this we first calculated the spin-averaged layer-resolved DOS (LRDOS) for all systems under investigation, as shown in Fig. 3. For the bulk spinel, the planes that pass through the Co-ions of corresponding charge state (A or B type) were used as for LRDOS calculations. All LRDOSs there are aligned in such a way that the highest filled states (Fermi level) are at zero energy. For the top layer of Co-terminated surfaces, there is clear evidence of such surface states present in the DOS (upper panels on Fig. 3, denoted “surface”). It contains a lot of features, not present in the bulk, and such a picture, in principle, is typical for all the considered surfaces with the dangling bonds. There is a notable difference in Co-terminated surface DOS for octahedral and tetrahedral termination at the region -18 eV, due to the oxygen atom shift from layer 2 and now belonging to the top layer of octahedral system. On the other hand,

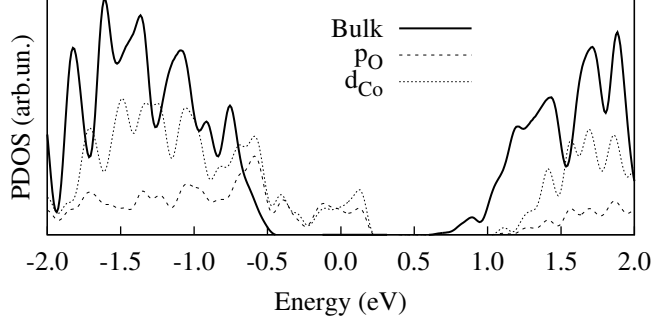


FIG. 4. Projected LRDOS for top layer of octahedral interface and octahedral plane of bulk spinel. The plot demonstrates domination of the p - and d -components of the wave function, while the s -state contributions can be neglected.

in tetrahedral system top layer consists of Co atoms only. LRDOS of O-terminated surfaces (not shown) demonstrates no noticeable difference, compared to the Co-terminated surface for both tetrahedral and octahedral coordinations. In this case, for both coordinations, the bonds of surface Co atoms now are passivated by oxygen atoms and are not broken anymore. This means, that there are also other factors responsible for the formation of the inside band-gap states. Such a situation is also observed in the case of interface. One can see from Fig. 3 (panels denoted “Layer n ” with $n=1, 2, 3,$ and 4), that LRDOS for the first layer demonstrates surface-like states inside the band-gap, close to the top of the valence band. For the internal layers these surface-like states are decaying with depth, and almost disappearing at Layer 4. Corresponding LRDOS becomes bulk-like, both for octahedral and tetrahedral coordinations, as seen from the comparison between LRDOS of Layer 4 and those denoted “Bulk” on Fig. 3.

Comparing LRDOS calculated for surface and interface, one can conclude, that although each Co-ion at the interface layer keeps the symmetry of the bulk crystalline environment, the physical properties of the interface region is closer to the surface, rather than to the bulk. To understand the origin of the surface-like states in the band-gap, we calculated the LRDOS of the octahedral interface, projected onto atomic wavefunctions of corresponding Co atom (s and d orbitals) and O atom (s and p orbitals), localized at the octahedral interface, as shown in Fig. 4. For convenience, we plotted there also LRDOS for A-plane of bulk spinel. As it can be seen, surface-like states originate predominantly from O $2p$ states and Co $3d$ states, while the contribution of s -states of both Co and O is negligibly small here.

Similar conclusions for the origin of the surface states in the tetrahedral systems have been also obtained. From this we conclude that charge state of Co-ion is not decisive in defining the surface or interface magnetism since in both of cases p -orbitals of O-atoms make the same contribution into DOS. Moreover, from the band structure calculation we see that the partial occupied states are common for all of the surfaces and interfaces under investigation. This demonstrates the metal-like electronic structure, in contrast to the bulk spinel, which appears semiconducting in the simulations even when larger smearing parameters in the Brillouin zone integration are used.

V. CONCLUSION

We investigated the origin of the surface/interface magnetism of the cobalt oxide Co_3O_4 surfaces and their interfaces with zinc oxide ZnO. In particular, we studied the structural, electronic and magnetic properties using the model systems such as $\text{ZnO}(0001)/\text{Co}_3\text{O}_4(111)$ interfaces, $\text{Co}_3\text{O}_4(111)$ surfaces for A-type and B-type terminations and bulk spinel. It is shown that while the magnetic moment of Co^{3+} ions is zero in the bulk, it does not vanish at the interface or surface, where its value becomes comparable with the magnetic moment of Co^{2+} due to the created imbalance in the electron distribution. The calculated LRDOS demonstrates that although Co ions at the interface have the same neighboring atoms as in bulk spinel, their DOS exhibit the surface-like nature, arising from polarized Co $3d$ and O $2p$ orbitals of the interfacing layer. In all cases, interface or surface, A- or B-type termination, we observe metallic-like states, localized at the surface or interface, and which are responsible for the surface/interface magnetism. Whereas the magnetic order is antiferromagnetic in the bulk spinel at low temperature, the metallic surface/interface states indicate the possibility of a ferromagnetic order at the surfaces or interfaces. The proposed mechanisms offer possible interpretation of the experimental observation of the net magnetic moment in certain Co doped ZnO with high Co concentrations.

ACKNOWLEDGMENTS

We thank O. Kolomys and V. Strelchuk for usefull discussions. The work was supported by Science for Peace and Security Program (the grant NATO NUKR.SFPP 984735). I.

Kupchak acknowledges EC for the RISE Project CoExAN GA644076 within HORIZON2020 program. The CPU time was provided by the Shared Hierarchical Academic Research Computing Network (Sharcnet) of Ontario, Canada.

REFERENCES

- ¹F. Matsukura, H. Ohno, A. Shen, and Y. Sugawara, *Phys. Rev. B* **57**, R2037 (1998).
- ²K. Olejník, M. H. S. Owen, V. Novák, J. Mašek, A. C. Irvine, J. Wunderlich, and T. Jungwirth, *Phys. Rev. B* **78**, 054403 (2008).
- ³T. Dietl, H. Ohno, F. Matsukura, J. Cibert, and D. Ferrand, *Science* **287**, 1019 (2000).
- ⁴H.-J. Lee, S.-Y. Jeong, C. R. Cho, and C. H. Park, *Appl. Phys. Lett.* **81**, 4020 (2002).
- ⁵K. Sato and H. Katayama-Yoshida, *Jpn. J. Appl. Phys.* **40**, L334 (2001).
- ⁶P. Sati, R. Hayn, R. Kuzian, S. Régnier, S. Schäfer, A. Stepanov, C. Morhain, C. Deparis, M. Laügt, M. Goiran, and Z. Golacki, *Phys. Rev. Lett.* **96**, 017203 (2006).
- ⁷S. Stefanowicz, G. Kunert, C. Simserides, J. A. Majewski, W. Stefanowicz, C. Kruse, S. Figge, T. Li, R. Jakiela, K. N. Trohidou, A. Bonanni, D. Hommel, M. Sawicki, and T. Dietl, *Phys. Rev. B* **88**, 081201 (2013).
- ⁸G. D. Nipan, V. A. Ketsko, T. N. Kol'tsova, A. I. Stognii, K. I. Yanushkevich, V. V. Pan'kov, A. M. Khoviv, and A. M. Solodukha, *Russ. J. Phys. Chem.* **51**, 1961 (2006).
- ⁹Y. Wang, S. Yuan, Y. Song, L. Liu, Z. Tian, P. Li, Y. Zhou, Y. Li, and S. Yin, *Chin. Sci. Bull.* **52**, 1019 (2007).
- ¹⁰J.-j. Li, W.-c. Hao, H.-z. Xu, and T.-m. Wang, *J. Appl. Phys.* **105**, 053907 (2009).
- ¹¹H. Çolak and O. Türkoğlu, *J. Mater. Sci. Mater. Electron.* **26**, 10141 (2015).
- ¹²T. Dietl, T. Andrearczyk, A. Lipińska, M. Kiecana, M. Tay, and Y. Wu, *Phys. Rev. B* **76**, 155312 (2007).
- ¹³T. Dietl, K. Sato, T. Fukushima, A. Bonanni, M. Jamet, A. Barski, S. Kuroda, M. Tanaka, P. N. Hai, and H. Katayama-Yoshida, *Rev. Mod. Phys.* **87**, 1311 (2015).
- ¹⁴R. O. Kuzian, J. Richter, M. D. Kuz'min, and R. Hayn, *Phys. Rev. B* **93**, 214433 (2016).
- ¹⁵T. Dietl, T. Andrearczyk, A. Lipińska, M. Kiecana, M. Tay, and Y. Wu, *Phys. Rev. B* **76**, 155312 (2007).
- ¹⁶X. Wang, J. Xu, X. Yu, K. Xue, J. Yu, and X. Zhao, *Appl. Phys. Lett.* **91**, 031908 (2007).

- ¹⁷A. Walsh, S.-H. Wei, Y. Yan, M. M. Al-Jassim, J. A. Turner, M. Woodhouse, and B. A. Parkinson, *Phys. Rev. B* **76**, 165119 (2007).
- ¹⁸Y. Sharma, N. Sharma, G. V. Subba Rao, and B. V. R. Chowdari, *Adv. Funct. Mater.* **17**, 2855 (2007).
- ¹⁹M. Bajdich, M. García-Mota, A. Vojvodic, J. K. Nørskov, and A. T. Bell, *J. Am. Chem. Soc.* **135**, 13521 (2013).
- ²⁰H.-J. Kim and J.-H. Lee, *Sens. Actuator B-Chem.* **192**, 607 (2014).
- ²¹D. R. Miller, S. A. Akbar, and P. A. Morris, *Sens. Actuator B-Chem.* **204**, 250 (2014).
- ²²F. P. Netzer and A. Fortunelli, eds., *Oxide Materials at the Two-Dimensional Limit (Springer Series in Materials Science 234)* (Springer International Publishing, 2016).
- ²³W. Roth, *J. Phys. Chem. Solids* **25**, 1 (1964).
- ²⁴C. E. Rodríguez Torres, F. Golmar, M. Ziese, P. Esquinazi, and S. P. Heluani, *Phys. Rev. B* **84**, 064404 (2011).
- ²⁵J. Noh, O. I. Osman, S. G. Aziz, P. Winget, and J.-L. Brédas, *Chem. Mater.* **27**, 5856 (2015).
- ²⁶J. Hutchison and N. Briscoe, *Ultramicroscopy* **18**, 435 (1985).
- ²⁷D. Su, S. Dou, and G. Wang, *Sci. Rep.* **4**, 5767 (2014).
- ²⁸S. C. Petitto and M. A. Langell, *J. Vac. Sci. Technol. A* **22**, 1690 (2004).
- ²⁹J. Buršík, M. Soroka, R. Kužel, and F. Mika, *J. Solid State Chem.* **227**, 17 (2015).
- ³⁰P. Thurian, G. Kaczmarczyk, H. Siegle, R. Heitz, A. Hoffmann, I. Broser, B. Meyer, R. Hoffbauer, and U. Scherz, in *Defects in Semiconductors 18*, Materials Science Forum, Vol. 196 (Trans Tech Publications, 1995) pp. 1571–1576.
- ³¹P. Ferstl, S. Mehl, M. a. Arman, M. Schuler, a. Toghan, B. Laszlo, Y. Lykhach, O. Brummel, E. Lundgren, J. Knudsen, L. Hammer, M. a. Schneider, and J. Libuda, *J. Phys. Chem. C* **119**, 16688 (2015).
- ³²C. Vaz, V. Henrich, C. Ahn, and E. Altman, *J. Cryst. Growth* **311**, 2648 (2009).
- ³³S. Mehl, P. Ferstl, M. Schuler, A. Toghan, O. Brummel, L. Hammer, M. A. Schneider, and J. Libuda, *Phys. Chem. Chem. Phys.* **17**, 23538 (2015).
- ³⁴V. G. Hadjiev, M. N. Iliev, and I. V. Vergilov, *J. Phys. C: Solid State Phys.* **21**, L199 (1988).
- ³⁵D. Bekermann, A. Gasparotto, D. Barreca, C. Maccato, M. Rossi, R. Matassa, I. Cianchetta, S. Orlanducci, M. Kete, and U. L. Štangar, *Cryst. Growth Des.* **12**, 5118

- (2012).
- ³⁶A. Montoya and B. S. Haynes, *Chem. Phys. Lett.* **502**, 63 (2011).
- ³⁷J. Chen and A. Selloni, *J. Phys. Chem. Lett.* **3**, 2808 (2012).
- ³⁸S. Selcuk and A. Selloni, *J. Phys. Chem. C* **119**, 9973 (2015).
- ³⁹M. Wang and Q. Chen, *Chem. Eur. J.* **16**, 12088 (2010).
- ⁴⁰J. Chen and A. Selloni, *Phys. Rev. B* **85**, 085306 (2012).
- ⁴¹X.-L. Xu, Z.-H. Chen, Y. Li, W.-K. Chen, and J.-Q. Li, *Surf. Sci.* **603**, 653 (2009).
- ⁴²F. Zasada, W. Piskorz, and Z. Sojka, *J. Phys. Chem. C* **119**, 19180 (2015).
- ⁴³I. Kupchak and N. Serpak, *Ukr. J. Phys.* **62**, 615 (2017).
- ⁴⁴D. Bekermann, A. Gasparotto, D. Barreca, C. Maccato, E. Comini, C. Sada, G. Sberveglieri, A. Devi, and R. A. Fischer, *ACS Appl. Mater. Interfaces* **4**, 928 (2012).
- ⁴⁵X.-L. Xu, Z.-H. Chen, Y. Li, W.-K. Chen, and J.-Q. Li, *Surf. Sci.* **603**, 653 (2009).
- ⁴⁶T. K. Jana, A. Pal, and K. Chatterjee, *J. Alloys Compd.* **653**, 338 (2015).
- ⁴⁷S. Park, S. Kim, H. Kheel, and C. Lee, *Sens. Actuator B-Chem.* **222**, 1193 (2015).
- ⁴⁸M. S. Martín-González, M. a. García, I. Lorite, J. L. Costa-Krámer, F. Rubio-Marcos, N. Carmona, and J. F. Fernández, *J. Electrochem. Soc.* **157**, E31 (2010).
- ⁴⁹A. Quesada, M. A. García, M. Andrés, A. Hernando, J. F. Fernández, A. C. Caballero, M. S. Martín-González, and F. Briones, *J. Appl. Phys.* **100**, 1 (2006).
- ⁵⁰M. a. García, F. Jiménez-Villacorta, a. Quesada, J. De La Venta, N. Carmona, I. Lorite, J. Llopis, and J. F. Fernández, *J. Appl. Phys.* **107**, 1 (2010), 0912.3458.
- ⁵¹M. S. Martín-González, M. a. García, I. Lorite, J. L. Costa-Krámer, F. Rubio-Marcos, N. Carmona, and J. F. Fernández, *J. Electrochem. Soc.* **157**, E31 (2010).
- ⁵²S. A. Kulkarni, P. Sawadh, and P. K. Palei, *J. Korean Ceram. Soc.* **58**, 100 (2014).
- ⁵³T. I. Lee, S. H. Lee, Y.-D. Kim, W. S. Jang, J. Y. Oh, H. Baik Koo, C. Stampfl, A. Soon, and J. M. Myoung, *Nano Lett.* **12**, 68 (2012).
- ⁵⁴P. Giannozzi, S. Baroni, N. Bonini, M. Calandra, R. Car, C. Cavazzoni, D. Ceresoli, G. L. Chiarotti, M. Cococcioni, I. Dabo, A. D. Corso, S. de Gironcoli, S. Fabris, G. Fratesi, R. Gebauer, U. Gerstmann, C. Gougoussis, A. Kokalj, M. Lazzeri, L. Martin-Samos, N. Marzari, F. Mauri, R. Mazzarello, S. Paolini, A. Pasquarello, L. Paulatto, C. Sbraccia, S. Scandolo, G. Sclauzero, A. P. Seitsonen, A. Smogunov, P. Umari, and R. M. Wentzcovitch, *J. Phys. Condens. Matter* **21**, 395502 (2009).
- ⁵⁵J. P. Perdew, K. Burke, and M. Ernzerhof, *Phys. Rev. Lett.* **77**, 3865 (1996).

- ⁵⁶J. D. Pack and H. J. Monkhorst, Phys. Rev. B **16**, 1748 (1977).
- ⁵⁷M. Methfessel and A. T. Paxton, Phys. Rev. B **40**, 3616 (1989).
- ⁵⁸B. Dorado, G. Jomard, M. Freyss, and M. Bertolus, Phys. Rev. B **82**, 035114 (2010).
- ⁵⁹X. Xie, Y. Li, Z.-Q. Liu, M. Haruta, and W. Shen, Nature **458**, 746 (2009).
- ⁶⁰Y. Liu, G. Zhu, J. Chen, H. Xu, X. Shen, and A. Yuan, Appl. Surf. Sci. **265**, 379 (2013).
- ⁶¹T.-L. Phan, N. Nghia, and S. Yu, Solid State Commun. **152**, 2087 (2012).
- ⁶²A. Mock, R. Korlacki, C. Briley, D. Sekora, T. Hofmann, P. Wilson, A. Sinitskii, E. Schubert, and M. Schubert, Appl. Phys. Lett. **108**, 051905 (2016).
- ⁶³D. L. Rousseau, R. P. Bauman, and S. P. S. Porto, J. Raman Spectrosc. **10**, 253 (1981).
- ⁶⁴S. Baroni, S. de Gironcoli, A. Dal Corso, and P. Giannozzi, Rev. Mod. Phys. **73**, 515 (2001).